# Supplementary Information

## Burstein-Moss Effect Leads to an Unusual Suppression of Bipolar Conduction with Shrinking Bandgap

Chenxi Zhao,[1][†] Shengtao Cui,[2][†] Yuanlong Li,[1] Yunbo Wu,[2] Tongrui Li,[2] Kai Li,[1] Liang Sun, [1] Zhe Sun,[2] Chong Xiao,[1,*] and Yi Xie[1]

[1]*Hefei National Research Center for Physical Sciences at the Microscale, University of Science and Technology of China, Hefei, Anhui, 230026, P. R. China*

[2]*National Synchrotron Radiation Laboratory, University of Science and Technology of China, Hefei, Anhui 230029, P. R. China*

[†]These authors contributed equally to this work.
[*]Correspondence to: C. X. (cxiao@ustc.edu.cn)

# 1. Methods

***Synthesis***:  High-purity bismuth powder (Bi, 99.997%; Alfa Asear), tellurium powder (Te, 99.99%; Aladdin), selenium powder (Se, 99.99%; Aladdin), and indium powder (In, 99.99%; Aladdin) were weighed according to the composition of $Bi_{2-x}In_xTe_2Se$ (x = 0, 0.03, 0.04, 0.06, 0.12) in a glove box under argon protection. The elements were loaded in quartz tubes and then immediately sealed in vacuum to prevent the the oxidation of bismuth. The $Bi_{2-x}In_xTe_2Se$ single crystals ingots were synthesized via vertical Bridgman method. The samples were first slowly heated to 1073 K and melted for 12h, and then were slowly cooled to 983 K. After pulling the quartz tube at a rate of 1 mm/h for 120h, the furnace was cooled down to room temperature. All single crystals were cut within the effective conductivity range at the same middle section of the elongated single crystal ingots for subsequent testing. The slow pulling speed aims to obtain high-quality single crystals with fewer crystal steps on the cleavage surface to serve ARPES measurement, ensuring that in the beam region there is no crystal step and preventing the tests from being disturbed by crystals with different in-plane orientations. The samples for transport measurement did not undergo the slowly pulling process in case of the phase separation during the slowly pulling process. The ingots were broken down, hot-pressed, and cut and polished into regular shapes according to the in-plane direction. The sample used for measuring electrical conductivity and seebeck coefficient is approximately $10 \times 2 \times 2$ mm. The sample used for measuring thermal conductivity is approximately $10 \times 10 \times 1.5$ mm. The sample used for Hall measurements is around $5 \times 5 \times 0.3$ mm. The precision of the thickness measurements

of samples used in Hall measurement is ±0.001 mm, measured precisely with a micrometer screw (293-240-30, Mitutoyo Japan).

***Characterization***: The phase composition was characterized by X-ray diffraction (XRD; Rigaku TTR-III) with Cu Ka radiation ($\lambda$ = 1.54 Å). The composition was characterized by energy-dispersive spectroscopy (EDS) installed on Schottky field emission scanning electron microscopy (FESEM; Zeiss GEMINISEM 500). The infrared spectrum was conducted on Thermo Fisher Nicolet iS50 FTIR using the diffuse reflectance mode, which was equipped with an integrating sphere. The normalized absorbance was calculated by the measured reflectance using Kubelka-Munk theory[1, 2].

***ARPES Measurements***:  The ARPES measurements were performed at beamline 13U of National Synchrotron Radiation Laboratory. The single crystals are well cleaved in vacuum. The pressure of the analysis chamber is better than $5 \times 10^{-11}$ mbar. The measurement was conducted at room temperature. The testing photon energy is 13 eV. The samples tested in ARPES are around 1.5 mm × 1.5 mm, and the beam size is around 0.3 mm × 0.3 mm.

***Hall measurement***: The temperature-dependent carrier concentrations were measured by the Van der Pauw method using the AC field Hall effect measurement option (Lake Shore 8400 series, USA). The AC gain was selected as 48 dB. The lock-in mode was configured to a slow response mode, ensuring that the standard deviation of the voltage at each point was less than 0.1% of the primary voltage signal.

***Thermoelectric Transport Measurements***:  The measurements of the electrical

conductivity and seebeck coefficient were conducted in ZEM-3 instrument system under a low-pressure helium atmosphere. The thermal conductivity is calculated by the formula $\kappa = D\rho C_p$, where $D$ is the thermal diffusivity, $\rho$ is the sample density, and $C_p$ is the specific heat. The thermal diffusivity ($D$) was measured by using the laser flash diffusivity method (Netzsch, LFA467) in an argon atmosphere. The sample density was measured via Archimedes drainage method. The specific heat ($C_p$) was calculated by Dulong-Petit law.

*Calculation of the Pisarenko plot:* The fitted Pisarenko curve in Fig. 3(a) in the main text shows an extracted density-of-states effective mass $m_d{}^*$ of 0.99 $m_e$, which is calculated according to Equations S1-S4 for degenerate semiconductors as follows[3]

$$n = \frac{8\pi\sqrt{2}}{h^3}(k_B T m_d{}^*)^{\frac{3}{2}} F_{1/2}(\eta) \tag{S1}$$

$$S = \frac{k_B}{e}\left[\frac{2F_1(\eta)}{F_0(\eta)} - \eta\right] \tag{S2}$$

$$F_j(\eta) = \int_0^\infty \frac{\varphi^j}{1+e^{\varphi-\eta}}d\varphi \tag{S3}$$

$$n_H = \frac{4F_0^2(\eta)}{3F_{1/2}(\eta)F_{-1/2}(\eta)}n \tag{S4}$$

where $F_j(\eta)$ is the Fermi integral, $\eta$ is the reduced Fermi level ($\eta=E_F/k_B T$), , and $k_B$ is the Boltzmann constant.

*Calculation of the Lorentz factor and electronic thermal conductivity:* The electrical thermal conductivity ($\kappa_e$) is calculated from the formula

$$\kappa_e = L\sigma T \tag{S5}$$

where $L$ is the Lorentz factor[4]. The Lorentz factor is derived according to

$$L = \left(\frac{k_B}{e}\right)^2 \left(\frac{(r+7/2)F_{r+5/2}(\eta)}{(r+3/2)F_{r+3/2}(\eta)} - \left[\frac{(r+5/2)F_{r+3/2}(\eta)}{(r+3/2)F_{r+1/2}(\eta)}\right]^2\right) \tag{S6}$$

Engaged with the measured seebeck coefficient and Equations S2 and S4, supposed the acoustic phonon scattering ($r = -1/2$) is the main scattering mechanism, the value of the Lorentz factor could be obtained from Equation S6[5, 6].
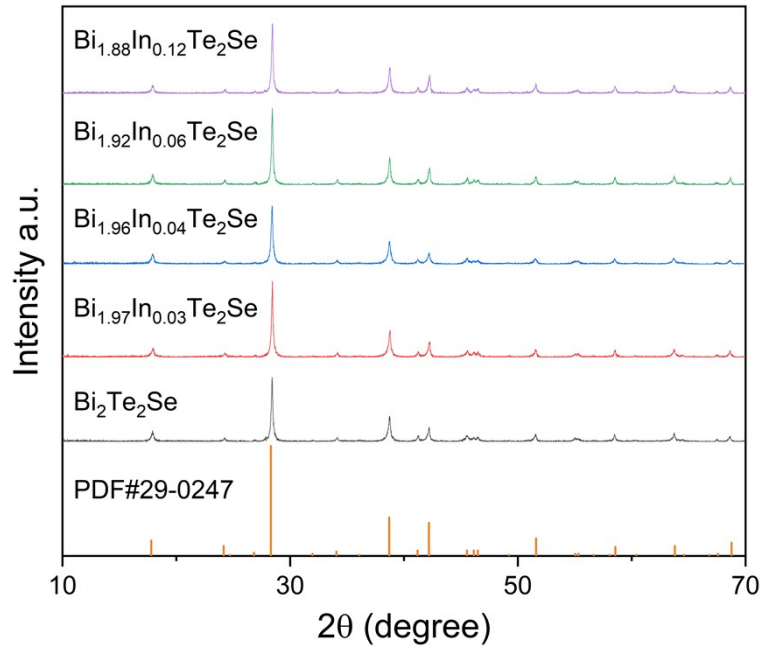
## 2. Supplemental data



**Fig. S1.** The XRD patterns of $Bi_{2-x}In_xTe_2Se$. The diffraction peaks from XRD patterns are consistent with those listed in JCPDS:29-0247, and no diffraction peaks from impurity phases were observed.
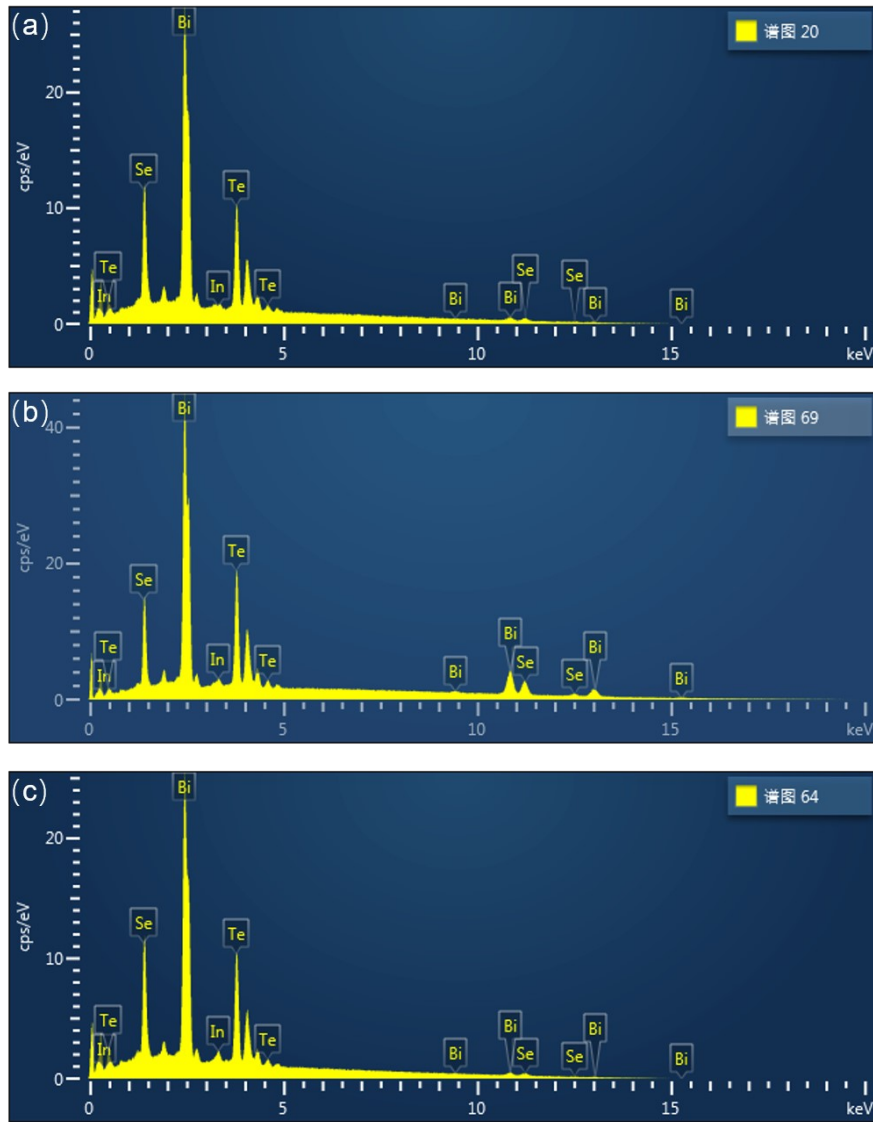
**Fig. S2.** The EDS diagrams of $Bi_{2-x}In_xTe_2Se$ samples used in ARPES measurements of (a) x = 0, (b) x = 0.06, and (c) x = 0.12, respectively.

**Table S1.** The composition of $Bi_{2-x}In_xTe_2Se$ samples used in ARPES measurements characterized by EDS. The EDS results show the homogenous composition of the solid-solution single crystal in ARPES measurements.

| | Point | Bi (%) | Te (%) | Se (%) | In (%) |
|---|---|---|---|---|---|
| x = 0 | point 1 | 41.36 | 35.24 | 23.40 | 0.00 |
| | point 2 | 41.41 | 35.37 | 23.22 | 0.00 |
| | point 3 | 41.14 | 35.84 | 23.03 | 0.00 |
| | point 4 | 41.58 | 35.80 | 22.61 | 0.00 |
| | point 5 | 41.17 | 35.79 | 23.03 | 0.00 |
| | average | 41.33 | 35.61 | 23.06 | 0.00 |
| | □ | □ | □ | □ | □ |
| x = 0.06 | point 1 | 39.87 | 35.94 | 22.91 | 1.29 |
| | point 2 | 40.35 | 36.47 | 21.88 | 1.30 |
| | point 3 | 40.10 | 35.98 | 22.77 | 1.14 |
| | point 4 | 40.15 | 36.10 | 22.73 | 1.02 |
| | point 5 | 39.87 | 36.29 | 22.77 | 1.06 |
| | average | 40.07 | 36.16 | 22.61 | 1.16 |
| | □ | □ | □ | □ | □ |
| x = 0.12 | point 1 | 38.54 | 36.83 | 22.31 | 2.32 |
| | point 2 | 38.78 | 36.60 | 22.50 | 2.13 |
| | point 3 | 38.47 | 36.46 | 22.74 | 2.32 |
| | point 4 | 38.33 | 36.57 | 22.81 | 2.30 |
| | point 5 | 38.47 | 36.50 | 22.63 | 2.40 |
| | average | 38.52 | 36.59 | 22.60 | 2.29 |
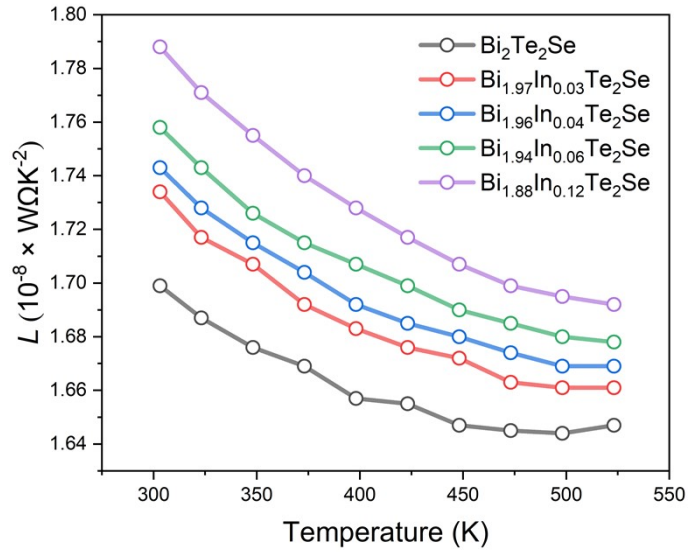
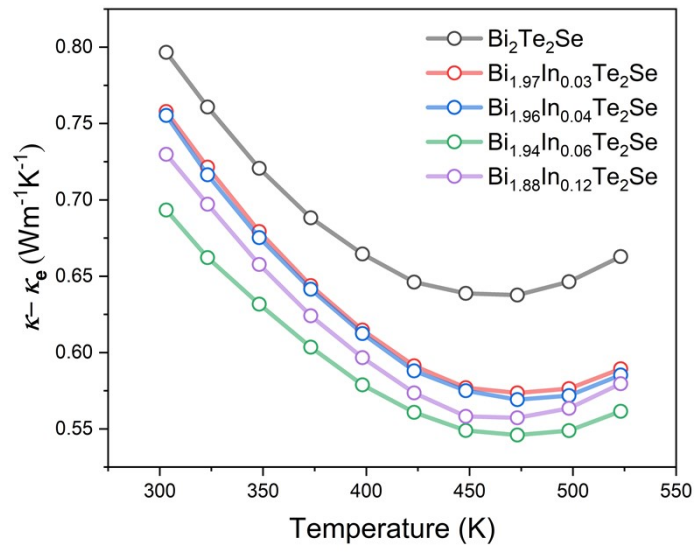**Fig. S3.** The temperature-dependent Lorentz factors of $Bi_{2-x}In_xTe_2Se$.

**Fig. S4.** The temperature-dependent difference between thermal conductivity and electronic thermal conductivity of $Bi_{2-x}In_xTe_2Se$.

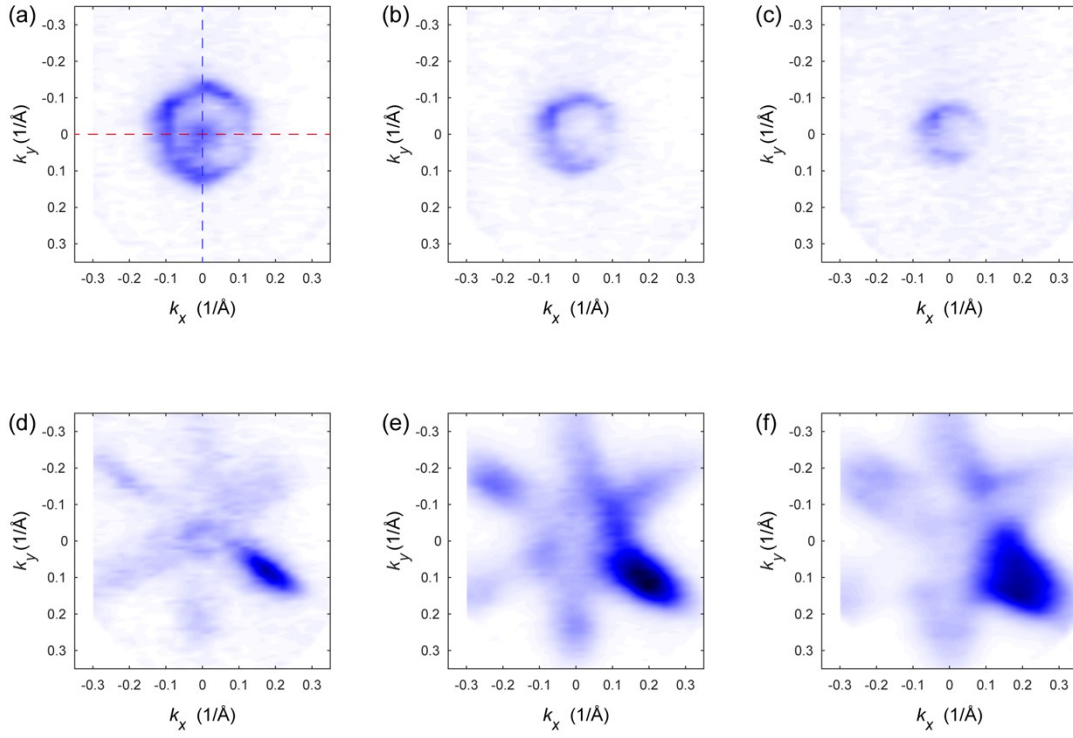**Fig. S5.** (a)–(f) ARPES maps of $Bi_2Te_2Se$ with binding energy ($E - E_F$) equals to (a) 0 eV, (b) 0.1 eV, (c) 0.2 eV, (d) 0.3 eV, (e) 0.4 eV, and (f) 0.5 eV, respectively. The blue dashed line in (a) represents the direction of $\bar{M} - \bar{\Gamma} - \bar{M}$. The red dashed line in (a) represents the direction of $\bar{K} - \bar{\Gamma} - \bar{K}$.
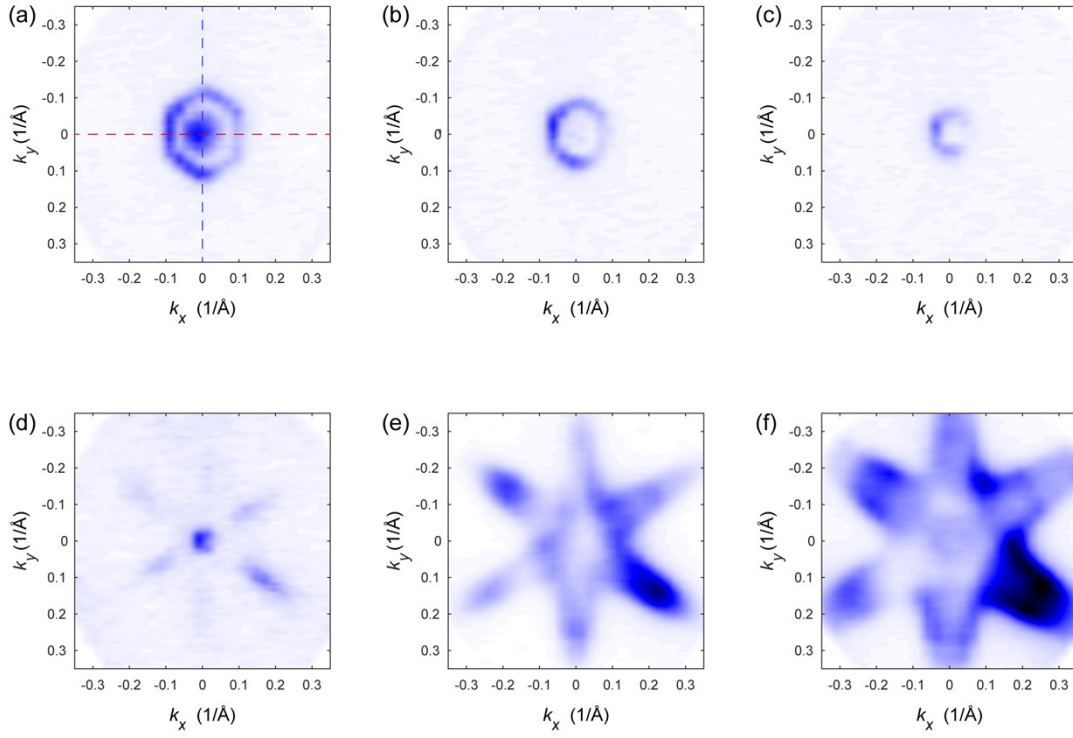
**Fig. S6.** (a)–(f) ARPES maps of $Bi_{1.94}In_{0.06}Te_2Se$ with binding energy ($E - E_F$) equals to (a) 0 eV, (b) 0.1 eV, (c) 0.2 eV, (d) 0.3 eV, (e) 0.4 eV, and (f) 0.5 eV, respectively. The blue dashed line in (a) represents the direction of $\bar{M} - \bar{\Gamma} - \bar{M}$. The red dashed line in (a) represents the direction of $\bar{K} - \bar{\Gamma} - \bar{K}$.
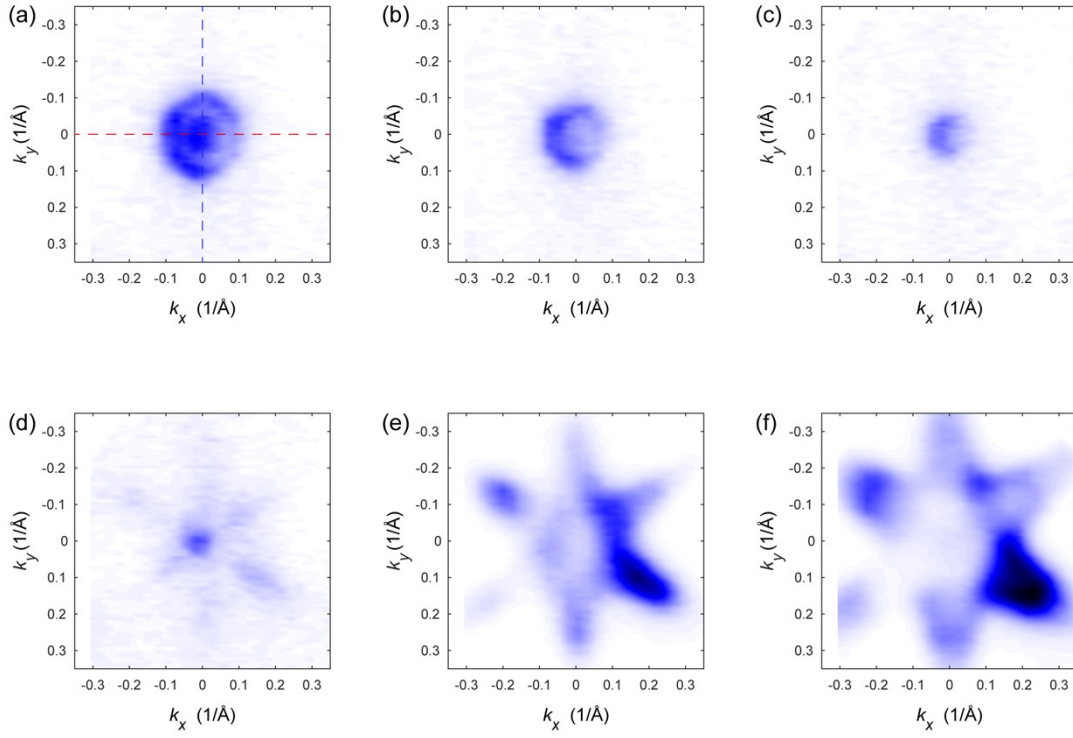
**Fig. S7.** (a)–(f) ARPES maps of $Bi_{1.88}In_{0.12}Te_2Se$ with binding energy ($E - E_F$) equals to (a) 0 eV, (b) 0.1 eV, (c) 0.2 eV, (d) 0.3 eV, (e) 0.4 eV, and (f) 0.5 eV, respectively. The blue dashed line in (a) represents the direction of $\bar{M} - \bar{\Gamma} - \bar{M}$. The red dashed line in (a) represents the direction of $\bar{K} - \bar{\Gamma} - \bar{K}$.

**Table S2.** The density and relative density of $Bi_{2-x}In_xTe_2Se$ samples conducted in transport measurements.

| x | Density (g/cm³) | Relative Density |
|---|---|---|
| 0 | 7.30 | 92.3% |
| 0.03 | 7.33 | 92.6% |
| 0.04 | 7.61 | 96.2% |
| 0.06 | 7.68 | 95.3% |
| 0.12 | 7.49 | 94.3% |

# References

[1]   P. Kubelka, F. Munk, *Z. Tech. Phys* **1931**, 12, 259.

[2]   A. E. Morales, E. S. Mora, U. Pal, *Revista mexicana de física* **2007**, 53, 18.

[3]   G. J. Snyder, A. Pereyra, R. Gurunathan, *Advanced Functional Materials* **2022**, 32, 2112772.

[4]   G. J. Snyder, E. S. Toberer, *Nature Materials* **2008**, 7, 105.

[5]   Y.-L. Pei, J. He, J.-F. Li, F. Li, Q. Liu, W. Pan, C. Barreteau, D. Berardan, N. Dragoe, L.-D. Zhao, *NPG Asia Materials* **2013**, 5, e47.

[6]   J. L. Lan, Y. C. Liu, B. Zhan, Y. H. Lin, B. Zhang, X. Yuan, W. Zhang, W. Xu, C. W. Nan, *Advanced Materials* **2013**, 25, 5086.